LETTERS

nature biotechnology

Chemotherapy-resistant human AML stem cells home to and engraft within the bone-marrow endosteal region

Fumihiko Ishikawa[1,3], Shuro Yoshida[1,3], Yoriko Saito[1,5], Atsushi Hijikata[2], Hiroshi Kitamura[2], Satoshi Tanaka[6], Ryu Nakamura[7], Toru Tanaka[7], Hiroko Tomiyama[6], Noriyuki Saito[3], Mitsuhiro Fukata[3], Toshihiro Miyamoto[4], Bonnie Lyons[8], Koichi Ohshima[9], Naoyuki Uchida[10], Shuichi Taniguchi[10], Osamu Ohara[2,11], Koichi Akashi[4,12], Mine Harada[3] & Leonard D Shultz[8]

Acute myelogenous leukemia (AML) is the most common adult leukemia, characterized by the clonal expansion of immature myeloblasts initiating from rare leukemic stem (LS) cells[1–3]. To understand the functional properties of human LS cells, we developed a primary human AML xenotransplantation model using newborn nonobese diabetic/severe combined immunodeficient/interleukin (NOD/SCID/IL)2rγ^{null} mice carrying a complete null mutation of the cytokine γc upon the SCID background[4]. Using this model, we demonstrated that LS cells exclusively recapitulate AML and retain self-renewal capacity *in vivo*. They home to and engraft within the osteoblast-rich area of the bone marrow, where AML cells are protected from chemotherapy-induced apoptosis. Quiescence of human LS cells may be a mechanism underlying resistance to cell cycle–dependent cytotoxic therapy. Global transcriptional profiling identified LS cell–specific transcripts that are stable through serial transplantation. These results indicate the potential utility of this AML xenograft model in the development of novel therapeutic strategies targeted at LS cells.

Although murine leukemia models have provided valuable insights into leukemogenesis, direct *in vivo* study of primary human leukemia is necessary to understand pathogenic mechanisms unique to human leukemogenesis[1]. However, existing immunodeficient strains such as CB17/SCID[5], NOD/SCID[6–8] and NOD/SCID/β2m^{null} (ref. 9) with short life spans and age-dependent leakiness of humoral immunity make long-term evaluation of primary human AML cell biology challenging. We recently created an immunodeficient strain with improved long-term xenogeneic engraftment, NOD.Cg-*Prkdc*^{scid}*Il2rg*$^{tm1Wjl/J}$ (NOD/SCID/IL2rγ^{null}), carrying a complete null mutation of the common γ chain[10]. This strain, with life expectancy >90 weeks, is more robust than strains such as NOD/SCID[11] and NOD/SCID/β2m^{null} (ref. 12), allowing assessment of the capacity for reconstitution and lymphoid/myeloid differentiation of human long-term repopulating hematopoietic stem cells[4,13].

Primary human AML cells engraft with high efficiency in the newborn NOD/SCID/IL2rγ^{null} model. We intravenously injected 4×10^6 T-cell–depleted bone-marrow mononuclear cells (BMMNCs) containing 80–90% leukemic myeloblasts, obtained from the bone marrow of nine people, into sublethally irradiated mice. Engraftment of the human cells occurred in significantly ($P = 0.0011$) more newborn NOD/SCID/IL2rγ^{null} recipients (37.8%) compared with adult NOD/SCID/IL2rγ^{null} (11.9%) and newborn NOD/SCID/β2m^{null} (12.9%) recipients (**Supplementary Fig. 1** online).

In CB17/SCID and NOD/SCID mice, engraftment of human hCD34$^+$hCD38$^-$ LS cells in bone marrow has been previously demonstrated, whereas engraftment in the peripheral blood has been limited[5,8]. We detected dose-dependent peripheral-blood AML engraftment in newborn NOD/SCID/IL2rγ^{null} recipients after intravenous injection of as few as 10^3 sorted primary AML hCD34$^+$hCD38$^-$ cells with no exogenous cytokine treatment or other manipulations, whereas injection of 5×10^4–10^6 hCD34$^+$hCD38$^+$ or 10^6 hCD34$^-$ cells resulted in no detectable engraftment (**Fig. 1a** and **Supplementary Table 1** online). Transplanted hCD34$^+$hCD38$^-$ LS cells gave rise to hCD45$^+$hCD34$^+$hCD38$^-$ LS cells, as well as hCD45$^+$hCD34$^+$hCD38$^+$ and hCD45$^+$hCD34$^-$ non-stem AML cells, demonstrating the long-term engraftment and differentiation capacity of primary LS cells *in vivo*. In addition to better reproducing primary AML disease *in vivo*, the presence of circulating peripheral-blood AML cells allows examination of one person's AML cells over multiple time points in a single recipient—a substantial advantage of the newborn NOD/SCID/IL2rγ^{null} mouse model.

[1]Research Unit for Human Disease Models and [2]Laboratory for Immunogenomics, RIKEN Research Center for Allergy and Immunology, 1-7-22 Suehiro-cho Tsurumi-ku, Yokohama 230-0045 Japan. [3]Department of Medicine and Biosystemic Science, Kyushu University Graduate School of Medicine and [4]Center for Cellular and Molecular Medicine, Kyushu University Hospital, 3-1-1 Maidashi Higashi-ku, Fukuoka 812-8582 Japan. [5]Department of Pathology, Massachusetts General Hospital, Harvard Medical School, 55 Fruit Street, Boston, Massachusetts 02114, USA. [6]Nippon Becton Dickinson Company, 4-15-1 Akasaka Minato-ku, Tokyo 107-0052 Japan. [7]Carl Zeiss, 22 Honshio-cho, Shinjuku-ku, Tokyo 160-0003 Japan. [8]The Jackson Laboratory, 600 Main Street, Bar Harbor, Maine 04609, USA. [9]First Department of Pathology, Kurume University School of Medicine, 67 Asahi-cho, Kurume 830-0011 Japan. [10]Department of Hematology, Toranomon Hospital, 2-2-2 Toranomon Minato-ku, Tokyo 105-8470 Japan. [11]Department of Human Genome Technology, Kazusa DNA Research Institute, 2-6-7 Kazusa Kamatari, Kisarazu 290-0818 Japan. [12]Department of Cancer Immunology and AIDS, Dana-Farber Cancer Institute, Harvard Medical School, 44 Binney Street, Boston, Massachusetts 02115, USA. Correspondence should be addressed to F.I. (f_ishika@rcai.riken.jp).

Received 28 December 2006; accepted 24 September 2007; published online 21 October 2007; doi:10.1038/nbt1350

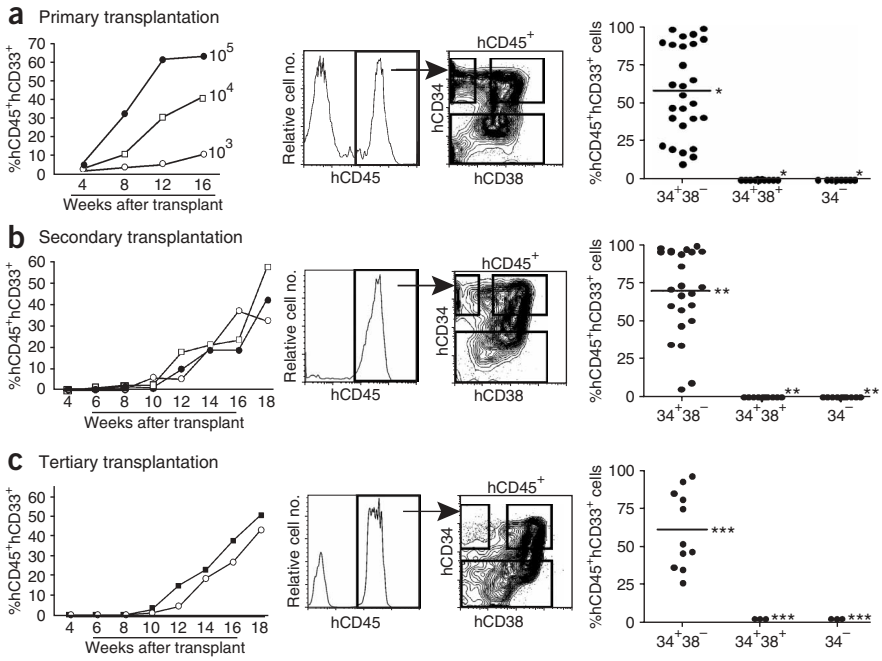

Figure 1 Self-renewing, long-term engrafting primary human LS cells reside exclusively within the hCD34$^+$hCD38$^-$ population. (**a**) Peripheral blood of primary recipients receiving 10^3, 10^4 or 10^5 sorted hCD34$^+$hCD38$^-$ cells analyzed 4, 8, 12 and 16 weeks after injection, showing dose-dependent engraftment (left panel). Primary recipient bone-marrow hCD45, hCD34 and hCD38 expression at 16 weeks (middle panel). Sorted primary recipient bone-marrow hCD34$^+$hCD38$^-$ cells (10^4) were injected into three secondary recipients. Summary of primary transplantation (rightmost panel). (**b**,**c**) Secondary (**b**) and tertiary (**c**) recipient peripheral-blood engraftment analyzed every 2 weeks between weeks 4 and 18 (left panels). Secondary recipient bone-marrow hCD45, hCD34 and hCD38 expression at 18 weeks (**b**, middle panel). Sorted secondary recipient bone-marrow hCD34$^+$hCD38$^-$ cells (8×10^3) were injected into two tertiary recipients. Tertiary recipient bone-marrow hCD45, hCD34 and hCD38 expression at 20 weeks (**c**, middle panel). Summary of peripheral-blood AML engraftment in sorted hCD34$^+$hCD38$^-$, hCD34$^+$hCD38$^+$ and hCD34$^-$ bone-marrow recipients at 16–24 weeks (rightmost panels). (*, and **, $P < 0.0001$; ***, $P < 0.005$; Kruskal-Wallis test. Open circle, filled circle and open square represent independent samples.

Serial transplantation of AML bone-marrow hCD34$^+$hCD38$^-$ cells demonstrated their self-renewal and differentiation capacities, which are defining properties of LS cells. Injection of as few as 10^4 and 10^3 purified AML bone-marrow hCD34$^+$hCD38$^-$ cells in secondary and tertiary recipients, respectively, resulted in successful long-term engraftment, giving rise to hCD34$^+$hCD38$^-$ cells and hCD34$^+$hCD38$^+$/hCD34$^-$ myeloblasts (**Fig. 1b**,**c**). As with primary recipients, all secondary and tertiary recipients of sorted hCD34$^+$hCD38$^-$ cells showed AML engraftment, whereas neither 5×10^4–10^6 hCD34$^+$hCD38$^+$ nor 10^5–2×10^6 hCD34$^-$ purified bone-marrow cells initiated leukemia detectable in secondary and tertiary recipients (**Supplementary Table 1**). These findings demonstrate that LS cells remain hCD34$^+$hCD38$^-$ during the course of serial transplantation and that the xenogeneic murine bone-marrow microenvironment successfully supports self-renewal and differentiation of human LS cells. Human AML was maintained cumulatively *in vivo* from the human donor to the mouse tertiary recipients for over 1 year, demonstrating the long-term self-renewal capacity of LS cells.

Normal human hematopoiesis was not observed in the course of serial transplantation, and recipient peripheral-blood erythrocytes and platelets were entirely of murine origin (data not shown). Furthermore, recipient peripheral-blood hemoglobin concentration and platelet counts were inversely proportional to the leukemic burden, mimicking the suppression of normal hematopoiesis characteristic of AML disease progression (**Fig. 2a**). Gross appearances of recipient femur and spleen confirmed suppressed erythropoiesis consistent with AML disease, findings not observed when sorted hCD34$^+$hCD38$^+$ and hCD34$^-$ AML or normal bone-marrow hCD34$^+$hCD38$^-$ cells were transplanted (**Fig. 2a**). Although recipient spleen size was variable among cases, spleens of all engrafted recipients contained human AML cells (data not shown). These findings provide additional functional evidence that LS cell engraftment and AML expansion in the NOD/SCID/IL2rγ^{null} mouse recapitulates human leukemogenesis.

The microenvironmental niche for human primary LS cells has not been defined *in vivo*. Successful long-term engraftment characterized by self-renewal of human LS cells and propagation of differentiated leukemic progeny demonstrates the capacity of NOD/SCID/IL2rγ^{null} bone marrow to provide a supportive microenvironment for human LS cell survival and AML expansion. Although *in situ* examination of human AML engraftment using a heterogeneous cell population has been reported[14], direct localization of the homing site of highly purified hCD34$^+$hCD38$^-$ LS cells has not been performed. To investigate the microenvironmental niche for human primary LS cells, we examined recipient femoral sections after intravenous LS cell injection. Three days after injection, hCD34$^+$ AML cells were found lining the endosteal surface, the site of the normal hematopoietic stem cell microenvironmental niche[15–17], whereas central regions of the bone marrow cavity were nearly acellular due to irradiation (**Fig. 2b**). hCD34$^+$hCD38$^-$ LS cells remain preferentially at the endosteal surface abutting murine osteoblasts 4 months after transplantation, when the bone marrow is packed with AML cells (**Fig. 2b**). Although the cells in the endosteal area were not morphologically uniform, not only round cells but also spindle-shaped cells expressed hCD45, demonstrating that they were human leukemic cells and not endothelial cells (**Fig. 2c**). Fluorescent *in situ* hybridization (FISH) analysis using mouse and human pancentromeric probes confirmed that these spindle-shaped cells were of human origin. Colocalization of hCD45 and hCD34 on the cells at the endosteal region was also demonstrated by confocal microscopy (**Supplementary Fig. 2** online). Quantitative analysis demonstrated that hCD34$^+$hCD38$^-$ LS cells homed to and continued to reside within the endosteal areas of the bone marrow (**Fig. 2d**). In people with AML, it is likely that the hCD34$^+$hCD38$^-$ population contains both normal hematopoietic stem cells and LS cells. However, the absence of normal hematopoietic engraftment of sorted hCD34$^+$hCD38$^-$ cells in NOD/SCID/IL2rγ^{null} mice indicates that the majority (either numerically or functionally) of these cells are of malignant origin. These findings suggest that the suppression of normal hematopoiesis during AML progression may result from the competition for the shared bone-marrow microenvironmental niche.

In vivo testing of therapeutic agents can facilitate the development and optimization of novel therapies for AML. We examined the *in vivo* anti-leukemic cytotoxicity of cytosine arabinoside (Ara-C), a standard chemotherapeutic agent for the treatment of AML, in AML-engrafted NOD/SCID/IL2rγ^{null} recipients (**Supplementary Fig. 3a** online). In Ara-C–treated mice, peripheral-blood AML burden was markedly reduced by day 8. The cytotoxic effect was accompanied by anemia and thrombocytopenia in all treated mice, with mild hepatic toxicity in one animal, consistent with the known toxicity profile of Ara-C (**Supplementary Fig. 3b**). As is the case in people with AML, the effect of a single round of Ara-C treatment was transient, followed by AML relapse, as demonstrated by recovery of the peripheral-blood AML cell count by days 16–28.

Using this therapeutic model, we examined the chemosensitivity of human AML stem and non-stem fractions. Flow cytometric analysis of bone marrow 3 d after Ara-C treatment revealed that the hCD34$^+$hCD38$^-$ LS cells were significantly ($P < 0.05$) more resistant to Ara-C compared with the non-stem AML fractions (**Fig. 3a**). To identify the location of chemotherapy-resistant leukemic cells, we performed hematoxylin-eosin and terminal deoxynucleotidyl transferase–mediated dUTP nick end labeling (TUNEL) using day 3, femoral bone sections 3 d after Ara-C treatment. This demonstrated a marked segregation of apoptotic cells in the central bone-marrow cavity from TUNEL-negative surviving cells lining the endosteal surface (**Fig. 3b**). Immunostaining confirmed that the cells abutting the endosteum expressed hCD34, but not hCD38, on their surface and were adjacent to osteopontin$^+$ osteoblasts (**Fig. 3c**). These spindle-shaped cells in the

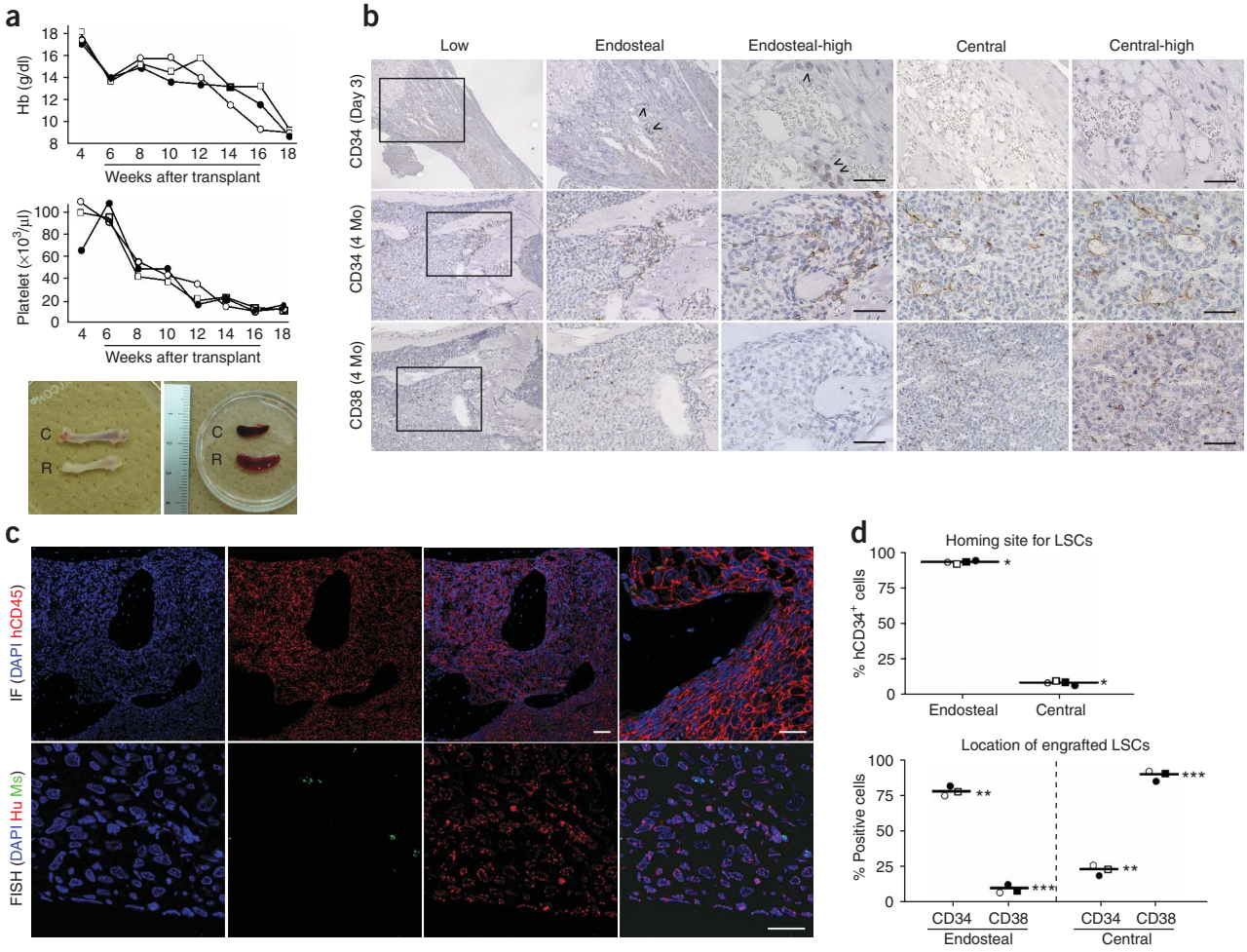

Figure 2 Primary human LS cells home to and engraft within the bone-marrow osteoblast-rich area, suppressing normal murine hematopoiesis. (**a**) Decline in peripheral-blood hemoglobin concentration (top) and platelet count (middle) with increasing human AML burden in the recipients of 10^4 sorted hCD34$^+$hCD38$^-$ bone-marrow cells (AML M2, $n = 3$). When compared with those of irradiated nontransplanted control mouse (C), femur and spleen of a recipient of bone-marrow LS cells at 18 weeks post-transplantation (R) show suppression of erythropoiesis (bottom). (**b**) Immunohistochemical analyses of femoral sections after hCD34$^+$hCD38$^-$ AML M4 bone-marrow cell homing (top panels). hCD34$^+$ AML cells (arrowheads) are present preferentially at the metaphyseal endosteal regions. Immunohistochemical analyses of AML M4 engrafted femur using anti-hCD34 (middle panels) and anti-hCD38 (bottom panels) antibodies. Scale bars, 20 μm. (**c**) (Upper panels) Bone sections of AML engrafted mice were labeled with anti-human CD45 antibody (red). Nuclei were labeled with DAPI (blue). Low and high magnification images are shown (scale bars, 50 μm and 20 μm, respectively). (Lower panels) Bone sections of AML engrafted mice were labeled with human pan-centromeric probe (red) and mouse pan-centromeric probe (green). Nuclei were labeled with DAPI (blue). Scale bars, 20 μm. (**d**) (Upper panel) Sites of LS-cell homing. In four independent samples, hCD34$^+$ cells were enumerated within the endosteal and the central areas of the bone marrow (* $P < 0.0001$, two-tailed *t*-test). (Lower panel) LS cell location in engrafted recipients. In three independent samples, hCD34$^+$ or hCD38$^+$ cells were enumerated within the endosteal and the central areas of the bone marrow (**, $P < 0.0001$, two-tailed *t*-test). Open circle, filled circle and open square represent independent samples.

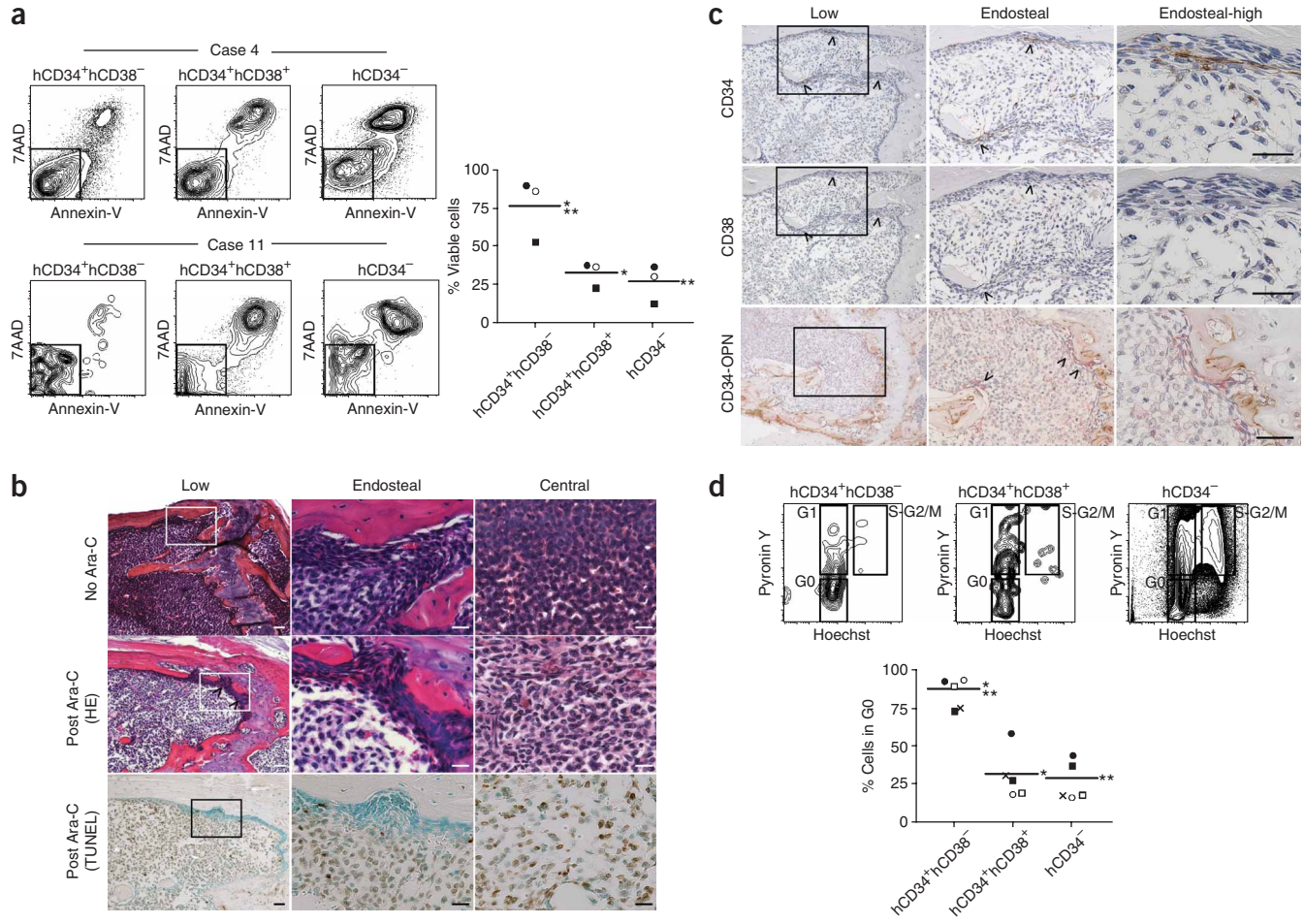

Figure 3 Primary hCD34$^+$hCD38$^-$ LS cells within the endosteal region exhibit relative resistance to Ara-C induced apoptosis. (**a**) Apoptosis analysis of LS cell and non-stem fractions from Ara-C–treated AML-engrafted mouse bone marrow ($n = 3$). Two sets of representative plots are shown (left panels). The hCD34$^+$hCD38$^-$ cells exhibit a relative resistance to Ara-C–induced apoptosis (right panel; *, ** $P < 0.05$, two-tailed *t*-test). Open circle, filled circle and open square represent independent samples. (**b**) Femoral bone from untreated and Ara-C-treated AML M2-engrafted mice. In the untreated femur, the bone marrow space is packed with AML blasts (upper panels; HE). At day 3 after Ara-C treatment, there is a decrease in cellularity in the bone marrow space except at the endosteal surface of the bone (middle panels; HE). TUNEL staining confirms the preferential killing of cells in the middle of the bone marrow cavity whereas the cells at the endosteal surface are relatively spared (lower panels). Low and high magnification images are shown (scale bars; 50 μm and 20 μm, respectively) (**c**) Immunohistochemical analyses of femoral bone section 3 d after Ara-C injection. Labeling with anti-hCD34 and anti-hCD38 antibodies show that hCD34$^+$hCD38$^-$ cells (arrowheads) remain in the endosteal region after chemotherapy (top and middle panels). Co-labeling with anti-hCD34 (pink) and anti-mOPN (brown) antibodies demonstrates that hCD34$^+$ AML cells (arrowheads) remain at the endosteal surface abutting murine osteoblasts (bottom panels). Scale bars, 20 μm. (**d**) Cell cycle status of LS cells and non-stem fractions in AML-engrafted recipients ($n = 5$). A representative set of plots is shown (upper panels). The majority of hCD34$^+$hCD38$^-$ LS cells is in the G_0 phase (lower panel; *, $P < 0.005$ and **, $P < 0.001$; two-tailed *t*-test).

endosteal region are human leukemic cells, not endothelial cells, as confirmed by hCD45 immunofluorescence labeling and dual FISH analysis (**Supplementary Fig. 4** online). Injection of 10^3 annexinV$^-$ 7AAD$^-$hCD34$^+$hCD38$^-$ cells from an Ara-C treated mouse resulted in AML engraftment in the secondary recipient, indicating that the chemoresistance of rare LS cells was responsible for AML relapse. Hoechst/pyronin Y staining demonstrated that hCD34$^+$hCD38$^-$ AML cells were cell-cycle quiescent compared with hCD34$^+$hCD38$^+$ and hCD34$^-$ cells (**Fig. 3d**). Because numerous chemotherapeutic agents, including Ara-C, exert cell cycle–dependent cytotoxicity, cell-cycle quiescence of LS cells may be one of the mechanisms underlying chemoresistance of LS cells.

Because LS cells exclusively initiate AML *in vivo* and are resistant to conventional chemotherapy, novel therapeutic strategies specifically targeting LS cells are needed to prevent disease relapse in human AML[18,19]. Recently, a cell-surface marker, CD44, was reported to be important both in mouse and human LS-cell homing and engraftment[20–22]. In addition to the prevention of AML initiation by interruption of LS-cell homing, it is imperative to develop therapies that eradicate LS cells that have already engrafted and give rise to non-stem AML cells. Comprehensive transcriptome analysis of primary AML LS cells compared with non-stem fractions is a useful tool to identify such LS cell–specific molecular targets at the level of the individual with AML. Our AML model facilitates such global gene profiling by providing LS cells and non-LS cells.

After prospective isolation of functionally defined LS cells from the bone marrow of four persons with primary AML and of the corresponding four recipient mice, we performed global gene expression profiling comparing hCD34$^+$hCD38$^-$ and hCD34$^+$hCD38$^+$ cells. Gene expression profiles of human donor bone marrow–derived and mouse

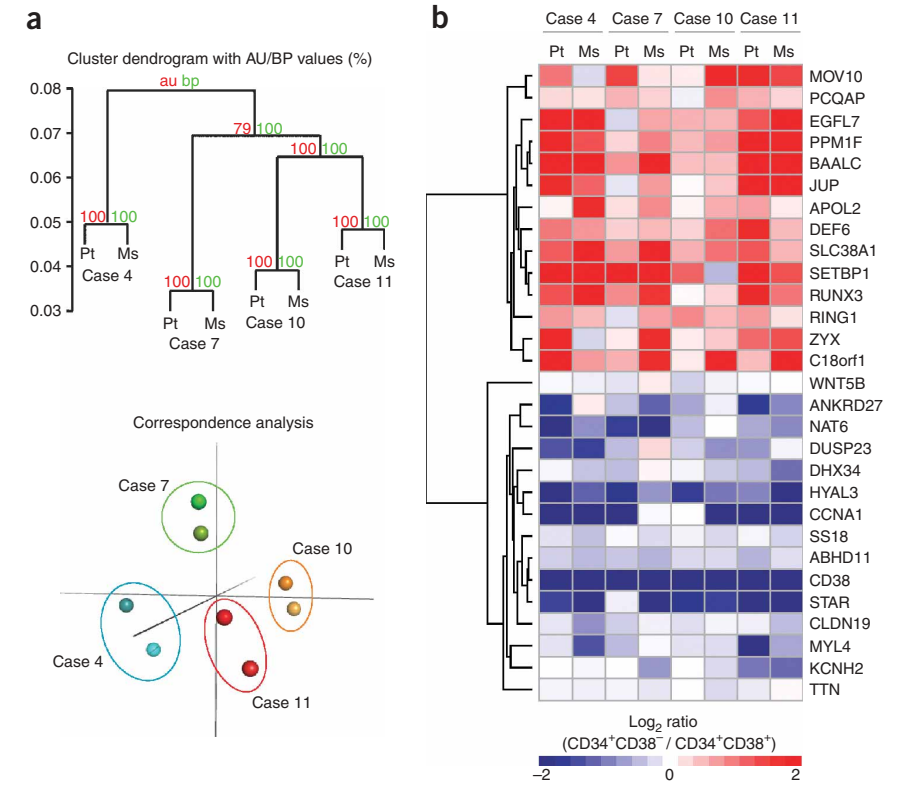

Figure 4 Global gene expression profiling of primary human AML and recipient mouse bone-marrow identifies LS cell–specific transcripts. (**a**) (Upper panel) Comparison of the global gene expression profiles between hCD34$^+$hCD38$^-$ cells derived from AML patient (Pt) and the corresponding recipient bone-marrow (Ms). This panel shows unsupervised hierarchical clustering using correlation distance and average linkage with assessment of the uncertainty in clustering by multiscale bootstrap resampling. The numbers at respective branches of the tree represent two types of *P*-values: approximately unbiased *P*-value (AU, red) and bootstrap probability value (BP, green). (Lower panel) Correspondence analysis independently demonstrates the statistically significant preservation of mRNA profile signatures of patient LS cells after long-term engraftment and serial transplantation in murine recipients. (**b**) Differentially expressed protein-coding genes between hCD34$^+$hCD38$^-$ and hCD34$^+$hCD38$^+$ cells with statistical significance. Fourteen and fifteen genes were significantly ($P < 0.01$) up- and downregulated, respectively, in hCD34$^+$hCD38$^-$ cells. The color scale indicates a Log_2 ratio of the normalized hybridization signal intensities of a differentially expressed gene in hCD34$^+$hCD38$^-$ cells to that in hCD34$^+$hCD38$^+$ cells. In this panel, red and blue display up- and downregulation in hCD34$^+$hCD38$^-$ cells, respectively, as shown in the reference color code at the bottom of the figure. Gene symbol for each differentially expressed gene identified is shown at the right of each row.

recipient bone marrow–derived hCD34$^+$hCD38$^-$ cells were highly correlated, indicating that gene expression signatures in LS cells remain relatively stable through serial transplantations in mouse bone-marrow microenvironment (**Fig. 4a**). This finding implies that the information derived from the analysis of recipient bone-marrow hCD34$^+$hCD38$^-$ cells correlates with that derived from human donor bone-marrow hCD34$^+$hCD38$^-$ cells. Therefore, we performed gene-set enrichment analysis to identify genes that are consistently enriched in hCD34$^+$hCD38$^-$ compared with hCD34$^+$hCD38$^+$ cells from each original primary AML bone marrow and the corresponding recipient bone marrow (**Supplementary Table 2** online). A gene set that was most significantly ($P = 0.000$, FDR q-value = 0.037) enriched in the LS cell fraction was the integrin pathway, including genes such as the *MAPKs*, *SRC* and *PXN*[23,24]. Signaling through these integrin-related genes leads to various downstream effects, including inhibition of apoptosis, cell cycle arrest in tumor cells, suppression of differentiation and expansion of the stem cell pool in normal epidermal cells (*SRC*, *MAPK*), promotion of squamous-cell carcinoma formation, control of immune cell migration and chemotactic responses (*FYN*), and regulation of cell adhesion and migration (*PXN*).

Furthermore, we identified genes that were differentially expressed, with statistical confidence, in LS cells by unsupervised hierarchical clustering (**Fig. 4b**). Those genes encode transcription factors, negative regulators of apoptosis and transmembrane molecules, potential targets for LS cell–specific therapy. Relative downregulation of *CCNA1*, which promotes cell cycle progression[25], is compatible with the increased G_0 frequency in LS cells demonstrated by cell cycle analysis (**Fig. 3d**). In contrast, *BAALC*[26], whose expression correlates with poor prognosis in AML, is highly expressed in LS cells. Additionally, *RING1*, which forms a polycomb complex through interaction with BMI-1 and acts as a transcriptional repressor, is also overexpressed in LS cells. Comprehensive transcriptome analysis that examines larger numbers of people with AML and compares functionally defined populations in NOD/SCID/IL2rγ^{null} mice is required for detection of LS cell–specific molecular targets in the future.

The NOD/SCID/IL2rγ^{null} model for engraftment of primary human AML cells provides insights into the biology of LS cells and allows us to answer questions previously unaddressed in existing SCID-repopulating models. Using this system, we demonstrated that (i) long-term engrafting, self-renewing LS cells are present in as few as 10^3 highly purified bone-marrow hCD34$^+$hCD38$^-$ cells, but not in hCD34$^+$hCD38$^+$ or hCD34$^-$ cells, from individuals with AML and from the engrafted recipient mouse; (ii) LS cells home to and expand within the osteoblast-rich endosteal area; (iii) the majority of LS cells are in the G_0 phase of the cell cycle, and are relatively resistant to Ara-C treatment, which contributes to AML relapse; (iv) LS cells engrafting in mouse bone marrow retain characteristics of human AML LS cells in phenotype, in function and in gene expression pattern, enabling the identification of novel LS cell–specific therapeutic targets in individuals with AML. The NOD/SCID/IL2rγ^{null} mouse may provide an *in vivo* model for determining the efficacy and optimal therapeutic window for treatment of AML in a patient-specific manner through prediction of the chemosensitivity of primary AML LS cells and evaluation of adverse effects of therapy. The model allows isolation of adequate numbers of rare LS cells with non-LS cell populations from recipient mice. The ability to expand primary LS cells *in vivo* enables large-scale molecular analysis of the LS cell transcriptome, facilitating discovery of therapeutic targets and analysis of drug resistance specific to LS cells for the development of patient-specific AML therapy targeted to LS cells.

METHODS

Mice. NOD.Cg-*Prkdc*^{scid}*Il2rg*^{tmlWjl}/Sz (NOD/SCID/IL2rγ^{null}) mice were developed at The Jackson Laboratory by backcrossing a complete null mutation[12]

at the *Il2rg* locus onto the NOD.Cg-*Prkdc*^{scid} (NOD/SCID) strain. NOD.Cg-*Prkdc*^{scid}*b2m*^{tm1Unc} (NOD/SCID/β2m^{null}) mice were obtained from a research colony maintained at The Jackson Laboratory. Mice were bred and maintained under defined flora with irradiated food and acidified water at the RIKEN animal facility and at The Jackson Laboratory, according to guidelines established by the Institutional Animal Committees at the respective institutions.

Human samples. All experiments were performed with authorization from the Institutional Review Board for Human Research at RIKEN RCAI and samples were collected from persons with AML with written informed consent. AML diagnoses included French-American-British (FAB) classification system subtype M1 (no maturation beyond promyelocytic; cases 1, 2 and 11), M2 (myeloblastic with maturation; cases 3, 4, 10), M3 (promyelocytic; cases 5, 6), M4 (myelomonocytic; cases 7, 8 and 12) and M7 (megakaryoblastic; case 9). BMMNCs were isolated using density-gradient centrifugation.

Primary and serial xenogeneic transplantation of primary AML BMMNCs. For T cell–depleted (TCD) BMMNC transplantation, whole BMMNCs were incubated with mouse anti-hCD3, hCD4, and hCD8 monoclonal antibodies (BD Immunocytometry), followed by T-cell removal with anti-mouse IgG antibody-conjugated immunomagnetic beads (Dynal). For sorted hCD34$^+$hCD38$^-$ AML cell transplantation, human AML BMMNCs were labeled with fluorochrome-conjugated mouse anti-hCD34 and anti-hCD38 monoclonal antibodies (BD Immunocytometry), followed by fluorescence-activated cell sorting (FACS) using FACSAria (Becton Dickinson). Doublets were excluded by analysis of FSC/SSC-height and FSC/SSC-width. The purity of hCD34$^+$hCD38$^-$ cells was >98% after sorting. Newborn (within 2 d of birth) and adult (10–12 weeks of age) mice received 100 and 300 cGy of total body irradiation, respectively, at 150 cGy/min using a ^{137}Cs-source irradiator, followed by intravenous injection of AML cells within 2 h.

For primary TCD-BMMNC transplantation, 4×10^6 cells from nine persons with AML (cases 1–9) were injected into irradiated recipients (newborn NOD/SCID/IL2rγ^{null}, adult NOD/SCID/IL2rγ^{null}, newborn NOD/SCID/β2m^{null}; n = 9 for each recipient strain) and BM AML engraftment was evaluated 3 months after transplantation. For primary purified cell transplantation, 10^3–2×10^5 hCD34$^+$hCD38$^-$, 5×10^4–10^6 hCD34$^+$hCD38$^+$ and 10^6 hCD34$^-$ bone-marrow AML cells from six people (cases 1, 4, 7, 10, 11 and 12) were injected into irradiated newborn recipients (n = 27, 12, 12, respectively) followed by peripheral-blood AML engraftment analysis every 4 weeks until 16–24 weeks after transplantation. Sixteen weeks after transplantation, primary recipients of 10^4 purified hCD34$^+$hCD38$^-$ AML cells from cases 1, 4, 7, 10 and 11 were killed and 10^4–5×10^5 hCD34$^+$hCD38$^-$, 5×10^4–10^6 hCD34$^+$hCD38$^+$ and 10^6 hCD34$^-$ FACS-purified primary bone-marrow cells were injected into irradiated secondary recipients (n = 24, 12, 12, respectively) followed by AML engraftment, hemoglobin concentration and platelet count analyses at 2–3 week intervals. Sixteen to 24 weeks after transplantation, secondary recipients of AML cases 4, 7 and 10 were killed and 10^3–10^5 hCD34$^+$hCD38$^-$, 5×10^4–10^6 hCD34$^+$hCD38$^+$ and 10^5–2×10^6 hCD34$^-$ FACS-purified bone-marrow cells were injected into irradiated tertiary recipients (n = 11, 3, 3, respectively) followed by AML engraftment, hemoglobin concentration and platelet count analyses at 2–4 week intervals until weeks 16–24.

Analysis of peripheral blood and bone marrow. Bone marrow was harvested from femurs and tibiae, and peripheral blood was collected from the retro-orbital plexus of recipients. Bone marrow and peripheral-blood cells were analyzed by FACSCanto II (BD) using mouse anti-hCD33, hCD13, hCD34, hCD38, hCD45, hGPA, hCD41a and rat anti-mTer119, and mCD41a monoclonal antibodies (BD Immunocytometry). Human AML engraftment in peripheral blood and bone marrow was defined as percentage of hCD45$^+$hCD33$^+$ MNCs in recipient peripheral blood and bone marrow, respectively, as all sorted hCD45$^+$hCD33$^+$ recipient MNCs were leukemic myeloblasts as confirmed by May-Grunwald-Giemsa staining (data not shown).

Histological analysis of NOD/SCID/IL2rγ^{null} recipient bone sections. Paraformaldehyde-fixed, decalcified, paraffin-embedded sections were prepared from femurs of the recipients transplanted with sorted hCD34$^+$hCD38$^-$ AML bone marrow cells. Immunohistochemical labeling was performed using mouse anti-hCD34 monoclonal (Immunotech), rabbit anti-hCD38 polyclonal (Spring Bioscience) and rabbit anti-mouse osteopontin (mOPN) monoclonal (Immuno-Biological Laboratories) antibodies as primary antibodies. Immunofluorescence labeling was performed using mouse anti-hCD45 monoclonal (Dako), mouse anti-hCD34 monoclonal (Immunotech), rabbit anti-mOPN monoclonal (Immuno-Biological Laboratories) and goat anti-hCD45 polyclonal (Santa Cruz Biotechnology) antibodies as primary antibodies. Dual FISH analyses were performed using Cy3-conjugated human pan-centromeric probe (Cambio) and FITC-conjugated mouse pan-centromeric probe (Cambio). Hematoxylin-eosin staining was performed using standard procedures. TUNEL staining was performed according to standard procedures using ApopTag peroxidase *in situ* apoptosis detection kit (Intergene). Light microscopy was performed using Zeiss Axiovert 200 (Carl Zeiss). Laser-scanning confocal imaging was obtained using Zeiss LSM *EXCITER* (Carl Zeiss).

Localization post-homing and post-engraftment. For quantitative localization of LS cells, enodosteal and central regions were defined as the zones within or outside twelve cells from the endosteum, respectively, as described previously[27]. Using immunohistochemically labeled bone sections as described above, hCD34$^+$ and hCD38$^+$ cells within each region were enumerated by light microscopy using Zeiss Axiovert 200. For homing analysis, 4×10^3–4×10^4 bone-marrow hCD34$^+$hCD38$^-$ cells from cases 4, 7 and 10 were injected into newborn recipients after receiving 6–8 Gy irradiation. The recipients were killed and femurs and tibiae were obtained for histological analyses on day 3. A total of 10,065 cells were counted from femoral and tibial sections. For post-engraftment localization analysis, a total of 24,973 cells were counted using femoral and tibial sections prepared from recipients of bone-marrow hCD34$^+$hCD38$^-$ cells from cases 4, 10 and 11, 16 weeks after transplantation.

Ara-C treatment and analysis. Intraperitoneal (i.p.) injection of 150 mg/kg Ara-C (Biogenesis) was performed in NOD/SCID/IL2rγ^{null} recipients transplanted with 10^4 purified bone-marrow hCD34$^+$hCD38$^-$ cells 12–16 weeks after transplantation. Peripheral blood was obtained at the time of injection (day 0) and every 4 d thereafter and MNCs were labeled with mouse anti-hCD45 and anti-hCD33 monoclonal antibodies to determine the fraction of hCD45$^+$hCD33$^+$ cells using flow cytometry. The number of AML cells/ml peripheral blood was determined by multiplying the fraction of peripheral-blood hCD45$^+$hCD33$^+$ cells by the total peripheral-blood leukocyte count/ml in each recipient. Hemoglobin concentration, platelet count and plasma aspartate aminotransferase (AST) levels were analyzed before and 8 d after Ara-C administration.

Post-chemotherapy apoptosis analysis. NOD/SCID/IL2rγ^{null} recipients transplanted with bone-marrow hCD34$^+$hCD38$^-$ cells from cases 4, 7 and 11, 12–20 weeks after transplantation were injected with 150 mg/kg Ara-C i.p. At day 3 after injection, bone marrow was analyzed for the presence of apoptotic cells by first dividing the hCD34$^+$hCD38$^-$, hCD34$^+$hCD38$^+$ and hCD34$^-$ fraction within the hCD45$^+$ gate and quantifying the viable population in each fraction by Annexin V and 7-amino-actinomycin D (7AAD) staining (BD Immunocytometry). Annexin V$^-$7AAD$^-$hCD45$^+$hCD34$^+$hCD38$^-$ cells were sorted and 10^3 cells were injected intravenously into irradiated newborn NOD/SCID/IL2rγ^{null} recipients.

Cell cycle analysis. NOD/SCID/IL2rγ^{null} recipients transplanted with bone-marrow hCD34$^+$hCD38$^-$ cells from cases 4, 7, 10 and 11, 12–20 weeks after transplantation were used for cell cycle analysis. For quantification of cells in G_0 phase of cell cycle, AML-engrafted recipient bone-marrow cells were labeled with Hoechst 33342 and pyronin Y followed by surface staining using anti-hCD34 and hCD38 antibodies using standard procedures.

Microarray analysis. For microarray analysis, 2–5×10^4 hCD34$^+$hCD38$^-$ and hCD34$^+$hCD38$^+$ cells were purified from people with AML and the corresponding secondary- or tertiary-recipient bone-marrow using FACSAria (total of four donor-recipient pairs). Total RNA was extracted using ISOGEN-LS reagent (Nippon Gene), and RNA integrity was assessed using a Bioanalyzer (Agilent). cDNA synthesis, aRNA amplification, biotinylation and fragmentation were performed with a One-Cycle Target Labeling Kit (Affymetrix). Fifteen μg of labeled samples was added to the hybridization cocktail, and

hybridized with Human Genome U133 Plus 2.0 GeneChips (Affymetrix) at 45 °C for 16 h as described by the manufacturer. Washing and streptavidin-phycoerythrin staining were conducted using a GeneChip Fluidics Station (Affymetrix). Subsequently, the chips were scanned using a GeneChip Scanner 3000 (Affymetrix). The normalized hybridization intensity for each probe set was calculated using the GC-RMA method[28] of the GeneSpring software package (Agilent) at the default setting. The microarray data were subjected to hierarchical clustering analysis using pvclust[29] implemented in R (http://www.r-project.org/) and the Gene Set Enrichment Analysis[28] using a "Curated" gene set collection built in February 2007 with the parameters at the default setting. Correspondence analysis using the same mRNA profiles was also performed[30]. To define genes showing significant differential expression between $CD34^+CD38^-$ and $CD34^+CD38^+$ cells, the microarray data were analyzed by statistical *t*-test with $P < 0.01$. In particular, human protein-coding genes in the RefSeq collection (http://www.ncbi.nlm.nih.gov/RefSeq/) were considered in this analysis.

Statistical analysis. The differences in mean percent engraftment was analyzed by the non-parametric Friedman two-way analysis of variance using BMDP Statistical Software (SPSS). The differences in mean percent primary and secondary engraftment of sorted populations were analyzed by the Kruskal-Wallis test (GraphPad Prism, GraphPad). Two-tailed *t*-test was used for homing and engraftment localization, apoptosis and cell cycle analyses (GraphPad Prism, GraphPad).

Accession codes. CIBEX: All the microarray data were deposited to CIBEX, a public gene-expression database in Japan, with an accession ID CBX21. 〈http://cibex.nig.ac.jp/〉

Note: Supplementary information is available on the Nature Biotechnology website.

ACKNOWLEDGMENTS

We thank T. Kanabayashi for the preparation of immunohistochemical staining; N. Aoki for assistance with bone sections; N. Suzuki for technical assistance; N. Kinukawa for assistance with statistical analysis; and F. Ishidate (Carl Zeiss) for assistance with microscopy. This work was supported by the Japan Ministry of Education, Culture, Sports, Science and Technology grant to F.I. and by the US National Institutes of Health grant to L.D.S.

AUTHOR CONTRIBUTIONS

F.I., overall experimental design, transplantation, data analysis, manuscript preparation and discussion; S.Y. transplantation and data analysis; Y.S. overall experimental design, data analysis, statistical analysis, manuscript preparation and discussion; A.H., microarray analysis; H.K., microarray analysis; S.T., flow cytometry; R.N., confocal imaging; T.T., confocal imaging; H.T., flow cytometry; N.S., data analysis; M.F., data analysis; T.M., discussion; B.L., data analysis; K.O., histological analysis; N.U., discussion; S.T., discussion; O.O., microarray analysis and discussion; K.A., discussion; M.H., discussion; L.D.S., discussion.

Published online at http://www.nature.com/naturebiotechnology
Reprints and permissions information is available online at http://npg.nature.com/reprintsandpermissions

1. Passegue, E., Jamieson, C.H., Ailles, L.E. & Weissman, I.L. Normal and leukemic hematopoiesis: are leukemias a stem cell disorder or a reacquisition of stem cell characteristics? *Proc. Natl. Acad. Sci. USA* **100** Suppl 1. 11842–11849 (2003).
2. Hope, K.J., Jin, L. & Dick, J.E. Acute myeloid leukemia originates from a hierarchy of leukemic stem cell classes that differ in self-renewal capacity. *Nat. Immunol.* **5**, 738–743 (2004).
3. Jordan, C.T. & Guzman, M.L. Mechanisms controlling pathogenesis and survival of leukemic stem cells. *Oncogene* **23**, 7178–7187 (2004).
4. Ishikawa, F. *et al.* Development of functional human blood and immune systems in NOD/SCID/IL2 receptor {gamma} chain(null) mice. *Blood* **106**, 1565–1573 (2005).
5. Lapidot, T. *et al.* A cell initiating human acute myeloid leukaemia after transplantation into SCID mice. *Nature* **367**, 645–648 (1994).
6. Bonnet, D. & Dick, J.E. Human acute myeloid leukemia is organized as a hierarchy that originates from a primitive hematopoietic cell. *Nat. Med.* **3**, 730–737 (1997).
7. Ailles, L.E., Gerhard, B. & Hogge, D.E. Detection and characterization of primitive malignant and normal progenitors in patients with acute myelogenous leukemia using long-term coculture with supportive feeder layers and cytokines. *Blood* **90**, 2555–2564 (1997).
8. Lumkul, R. *et al.* Human AML cells in NOD/SCID mice: engraftment potential and gene expression. *Leukemia* **16**, 1818–1826 (2002).
9. Feuring-Buske, M. *et al.* Improved engraftment of human acute myeloid leukemia progenitor cells in beta 2-microglobulin-deficient NOD/SCID mice and in NOD/SCID mice transgenic for human growth factors. *Leukemia* **17**, 760–763 (2003).
10. Cao, X. *et al.* Defective lymphoid development in mice lacking expression of the common cytokine receptor gamma chain. *Immunity* **2**, 223–238 (1995).
11. Shultz, L.D. *et al.* Multiple defects in innate and adaptive immunologic function in NOD/LtSz-scid mice. *J. Immunol.* **154**, 180–191 (1995).
12. Christianson, S.W. *et al.* Enhanced human CD4+ T cell engraftment in beta2-microglobulin-deficient NOD-scid mice. *J. Immunol.* **158**, 3578–3586 (1997).
13. Shultz, L.D. *et al.* Human lymphoid and myeloid cell development in NOD/LtSz-scid IL2R gamma null mice engrafted with mobilized human hemopoietic stem cells. *J. Immunol.* **174**, 6477–6489 (2005).
14. Ninomiya, M. *et al.* Homing, proliferation and survival sites of human leukemia cells in vivo in immunodeficient mice. *Leukemia* **21**, 136–142 (2007).
15. Zhang, J. *et al.* Identification of the haematopoietic stem cell niche and control of the niche size. *Nature* **425**, 836–841 (2003).
16. Calvi, L.M. *et al.* Osteoblastic cells regulate the haematopoietic stem cell niche. *Nature* **425**, 841–846 (2003).
17. Arai, F. *et al.* Tie2/angiopoietin-1 signaling regulates hematopoietic stem cell quiescence in the bone marrow niche. *Cell* **118**, 149–161 (2004).
18. Guzman, M.L. *et al.* The sesquiterpene lactone parthenolide induces apoptosis of human acute myelogenous leukemia stem and progenitor cells. *Blood* **105**, 4163–4169 (2005).
19. Taussig, D.C. *et al.* Hematopoietic stem cells express multiple myeloid markers: implications for the origin and targeted therapy of acute myeloid leukemia. *Blood* **106**, 4086–4092 (2005).
20. Charrad, R.S. *et al.* Ligation of the CD44 adhesion molecule reverses blockage of differentiation in human acute myeloid leukemia. *Nat. Med.* **5**, 669–676 (1999).
21. Jin, L., Hope, K.J., Zhai, Q., Smadja-Joffe, F. & Dick, J.E. Targeting of CD44 eradicates human acute myeloid leukemic stem cells. *Nat. Med.* **12**, 1167–1174 (2006).
22. Krause, D.S., Lazarides, K., von Andrian, U.H. & Van Etten, R.A. Requirement for CD44 in homing and engraftment of BCR-ABL-expressing leukemic stem cells. *Nat. Med.* **12**, 1175–1180 (2006).
23. Cursi, S. *et al.* Src kinase phosphorylates Caspase-8 on Tyr380: a novel mechanism of apoptosis suppression. *EMBO J.* **25**, 1895–1905 (2006).
24. Janes, S.M. & Watt, F.M. New roles for integrins in squamous-cell carcinoma. *Nat. Rev. Cancer* **6**, 175–183 (2006).
25. Ji, P. *et al.* Cyclin A1, the alternative A-type cyclin, contributes to G1/S cell cycle progression in somatic cells. *Oncogene* **24**, 2739–2744 (2005).
26. Tanner, S.M. *et al.* BAALC, the human member of a novel mammalian neuroectoderm gene lineage, is implicated in hematopoiesis and acute leukemia. *Proc. Natl. Acad. Sci. USA* **98**, 13901–13906 (2001).
27. Nilsson, S.K., Johnston, H.M. & Coverdale, J.A. Spatial localization of transplanted hemopoietic stem cells: inferences for the localization of stem cell niches. *Blood* **97**, 2293–2299 (2001).
28. Subramanian, A. *et al.* Gene set enrichment analysis: a knowledge-based approach for interpreting genome-wide expression profiles. *Proc. Natl. Acad. Sci. USA* **102**, 15545–15550 (2005).
29. Suzuki, R. & Shimodaira, H. Pvclust: an R package for assessing the uncertainty in hierarchical clustering. *Bioinformatics* **22**, 1540–1542 (2006).
30. Culhane, A.C., Thioulouse, J., Perriere, G. & Higgins, D.G. MADE4: an R package for multivariate analysis of gene expression data. *Bioinformatics* **21**, 2789–2790 (2005).